

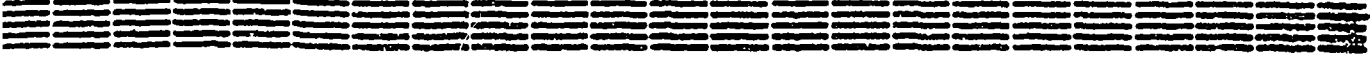
51

AM 96000/11

УЕКРHI

Preprint YPI-1301(11)-92

ԵՐԵՎԱՆԻ ՖԻԶԻԿԱՅԻ ԻՆՍՏԻՏՈՒՏ  
ЕРЕВАНСКИЙ ФИЗИЧЕСКИЙ ИНСТИТУТ  
YEREVAN PHYSICS INSTITUTE



Ts. A. Amatuni, E. A. Mamidjanjan and Kh. N. Sanossyan

Monte-Carlo Simulation of Hadronic Showers

Part 1: Comparison with Experiment

ЦНИИАтоминформ

Ереван 1992

VOL 27 № 2.2

**Յ. Ա. ԱՍԱՏՈՒՆԻ, Է. Ա. ՄԱՄԻՋԱՆՅԱՆ, Խ. Ն. ՍԱՆՈՍՅԱՆ**

**ՀԱԴՐՈՆԱՅԻՆ ՀԵՂԵՂՆԵՐԻ ԽԱՂԱՐԿՈՒՄԸ ՄՈՆՏԵ-ՔԱՐԼՈ ԵՂԱՆԱԿՈՎ**

**ՄԱՍ 1. MARS10 ԾՐԱԳՐԻ ՀԱԶՎԱՐԿՆԵՐԻ ՀԱՍԵՄԱՏՈՒԹՅՈՒՆԸ  
ԳԻՏԱՓՈՐՁԵՐԻ ԱՐԴՅՈՒՆՔՆԵՐԻ ՀԵՏ**

MARS10 ծրագրով [1] խաղարկված են հադրոնային հեղեղներ եւ կատարված են համեմատություններ բարձր էներգիայի արագացուցչային տարրեր գիտափորձերի արդյունքների հետ: Դիտվել են գիտափորձերի եւ խաղարկման արդյունքների լավ համանկումներ: MARS10-ն արագ եւ հուսալի միջոց է հադրոնային հեղեղների միջին բնութագրիչների թվային հետազոտման համար:

**ԵՐԵՎԱՆԻ ՏԻԶԻԿԱՏԻ ԻՆՍՏԻՏՈՒՏ**

**ԵՐԵՎԱՆ 1992**



## 1. Introduction

In the first part of this work we consider the comparison of results obtained by the MARSIO code with experimental data. In the subsequent parts we will discuss the results for various calorimetric devices which are operating or under construction in the world-wide energy range. It is worth to notice that the development of hadronic showers in condensed medium can be done, the help of MARSIO code was considered and discussed with reference [1], along the results of other authors with the purpose of demonstrating the ability of these codes. These are both differential and integral characteristics of hadronic showers which are in good agreement. A short review of results obtained using three different programs was published in [2], CABIN [3] and MARSIO [4] which are devoted to solve the design problems of calorimeters and accelerators, in the case of MARSIO [5]. The quantities used for comparison are the basic ones common to the output of these codes: the star density,  $S^*$ , and the energy deposition  $E_{dep}$ . As it is concluded in [5] the results agree very well for conditions and even a wide energy range. This is particularly true for the rather different sector: production and transport of particles.

The code was written at the Institute in mid 70-ies and has been extensively modified and tested by the IHEP (Serpukhov) people in the past years. A weighted Monte-Carlo algorithm is used in MARSIO, then only the average characteristics of the shower can be obtained. Typical computing times are of the order of an hour and increase logarithmically with the incident energy.

The purpose of the present work was mostly to familiarize ourselves with the MARSIO code in practice. We have simulated calorimetric experiments on the accelerators and made comparison of the results.

## 2. The Prototype of CHARM Calorimeter [6,7]

The layout of the calorimeter is given in fig. 1 (see ref.-s [6,7] for details). We have calculated pion induced longitudinal shower profiles in a Marble/Al/scintillator sandwich with a geometry corresponding to that presented in fig. 1. The experimental[7] and the calculated shower profiles for 1, 2, 3, 5 and 6 GeV pion induced showers are given in fig. 2. As it is seen from the figures the agreement is quite good.

## 3. The CDHS Calorimeter Prototype [8]

This is an Iron/Scintillator total absorption calorimeter. Figure 3 shows the details of its structure (see ref.[8]). We have calculated the development of hadronic showers initiated by 10 GeV pions for 10, 20 and 30 MeV energy cutoffs. The comparison between the experimental[8] and calculated shower profiles is shown in fig. 4. It can be seen, that the shower attenuation slope depends on this cutoff value. For 30 MeV cutoff the agreement with the experimental data is satisfactory.

It's worthwhile to mention that the value of the energy cutoff is to be adjusted empirically. There is no simple and direct connection between this Monte-Carlo cutoff and the actual cutoff imposed by the detection system.

## 4. The HEAD Calorimeter [9,10]

This was a Tungsten/Scintillator sandwich calorimeter designed for Mission A of HEAD. The prototype was exposed to particle beams at SLAC and FNAL. The arrangement of the apparatus in the experiment at SLAC is shown schematically in fig. 5 (for a detailed description see ref. [11,12]). The average number of equivalent particles has been calculated for 5, 10 and 15 GeV/c pion induced cascades. The comparison of our Monte-Carlo results with the experimental data in units of the average energy loss of sea-level cosmic ray muons is presented in fig. 6. As it is seen from the figure the agreement is good.

**POOR QUALITY  
ORIGINAL**

## 5. The Prototype of an Iron/Scintillator Sampling Total Absorption Detector for Neutrino Experiments at FNAL [13, 14]

The schematic view of the scaled-down calorimeter is shown in fig. 7. The experimental data[13,14] was obtained with a momentum and sign selected secondary beam, which at energies above 100GeV was primarily composed of hadrons(mostly protons and pions for positive sign selection and mostly pions for negative sign selection) with a small muon contamination.

In our Monte-Carlo calculation we used protons and positive pions with equal weight to simulate the case with positive hadrons and a pure beam of negative pions to simulate the negative hadrons. Proton and pion cascades do not differ drastically at high energies and the kaon contamination of the beam is supposed to be negligible, so this assumption is valid.

The fractional energy depositions along the calorimeter depth for 100, 200 and 250GeV negative hadrons are given in fig. 8, and that for 150 and 200GeV positive hadrons in fig. 9. The agreement with the experimental data[13,14] is satisfactory.

## 6. Iron and Lead Sandwiched with X-Ray Films [15]

The X-ray film chambers were exposed in the 300GeV proton beam at CERN[15]. The schematic view of the chamber is shown in fig. 10(see ref. [15] for details).

Our calculations of the longitudinal development of 300GeV proton induced cascades in the iron absorber are in a good agreement with the experimental curves from ref. [15], which are given in fig. 11 a). There is a disagreement between the calculated and the experimental profiles for 300GeV proton induced cascades in lead absorber(see fig. 11 b). As it can be seen from the figure the Monte-Carlo curve is systematically higher by a factor of about 1.5. Variation of the Monte-Carlo energy cutoff from 10MeV to 50GeV does not change the situation.

The lateral development of the same cascades were also analysed. The calculated and the experimentally measured longitudinal profiles for various distances from the shower axis are given in fig. 12(iron absorber) and fig. 13(lead absorber). Here also the Monte-Carlo results are in good agreement with the experimental data for the case of the iron absorber, while for the lead absorber the agreement is unsatisfactory. This circumstance is also noted by the authors of ref. [16] using a different Monte-Carlo code.

## 7. CONCLUSION AND ACKNOWLEDGEMENTS

The comparison of the experimental data and the results obtained using MARS10 code shows good agreement. MARS10 is a fast and reliable instrument for numerical studies of the average characteristics of hadronic showers.

We would like to thank N. Mokhov and A. Uzunyan from IHEP(Serpukhov) who made available for us the 10-th version of MARS. We would like to thank also our numerous friends and colleagues from the Cosmic Ray Department of YerPI for many useful and stimulating discussions. Last but not least, our acknowledgements go also to A. Adjemyan, N. Akopov and H. Harutunyan from the YerPI computer center.

We would like to express our deep gratitude to Archbishop Garegin Kersissian - Primate of the Araratyan Patriarchal Diocese for his kind permission to use the text processing utilities of the Armenian Church Youth Organization.

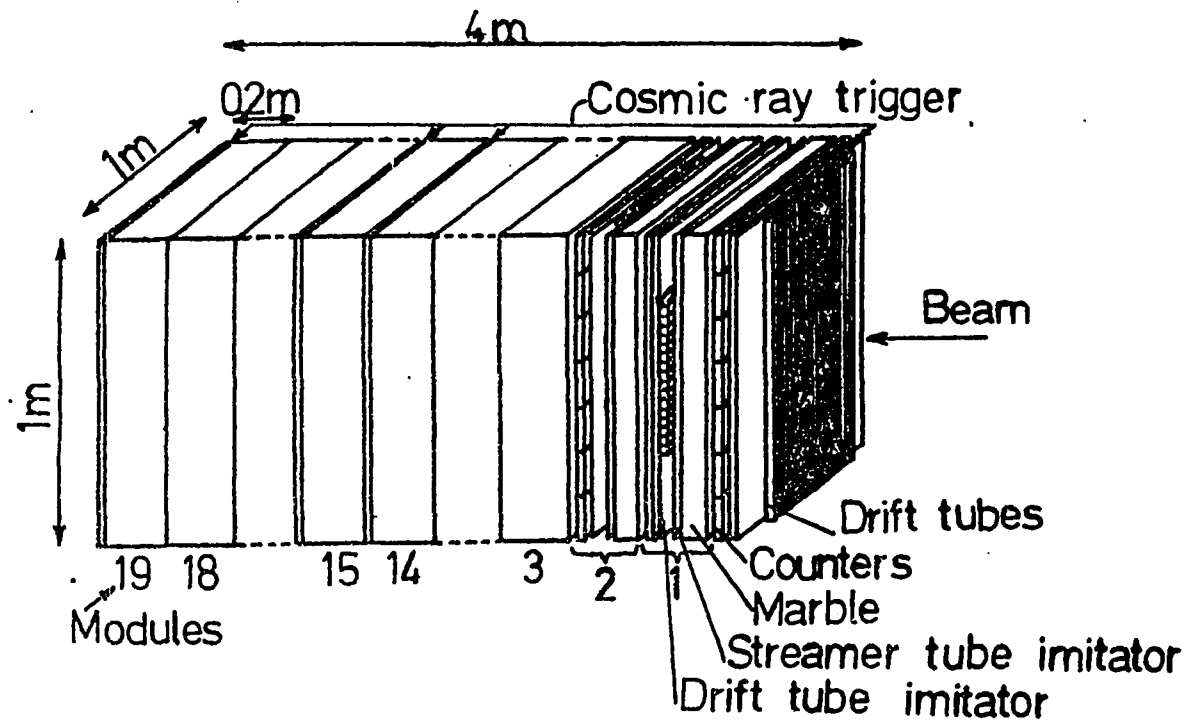


Fig. 1.1

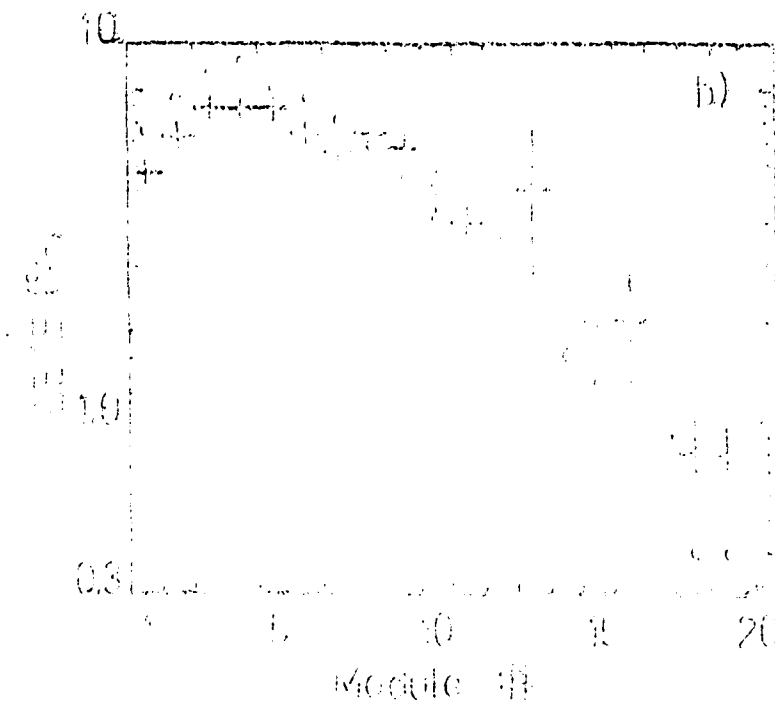
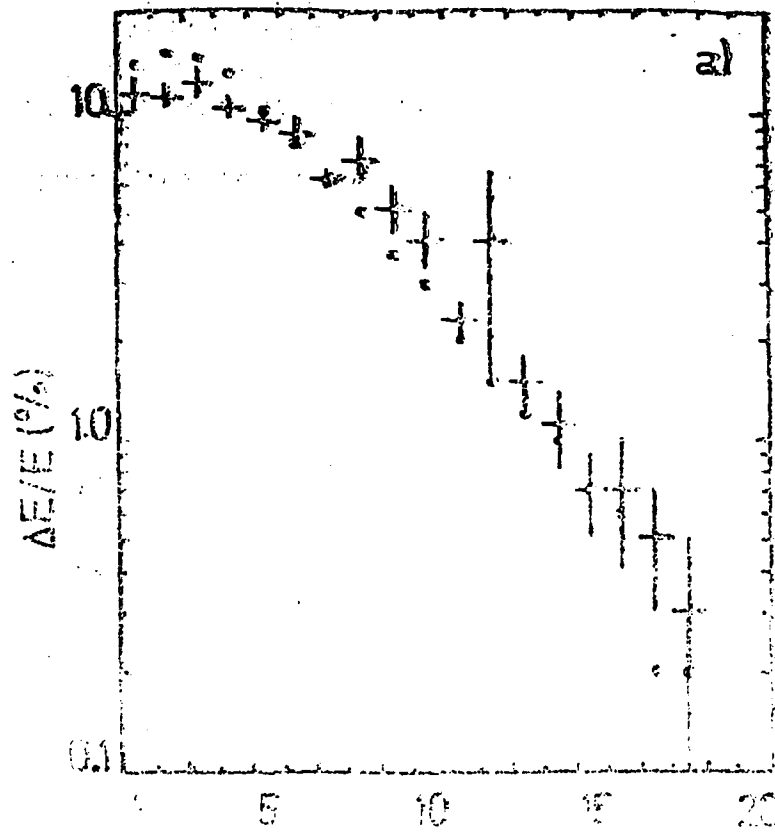


Fig. 12



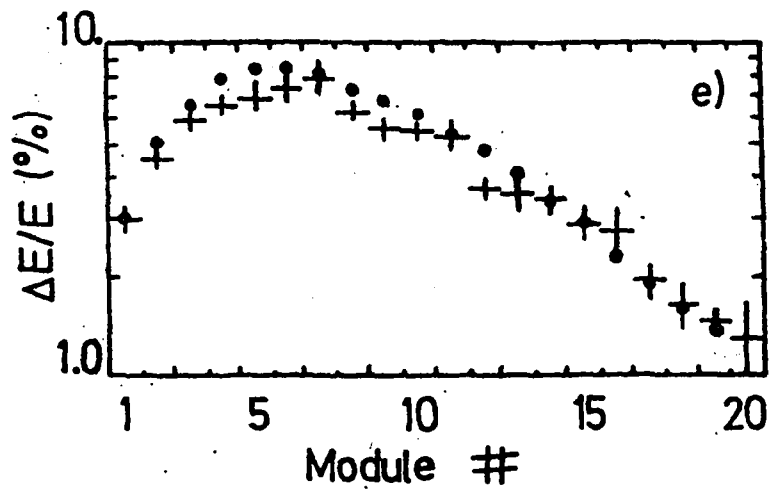
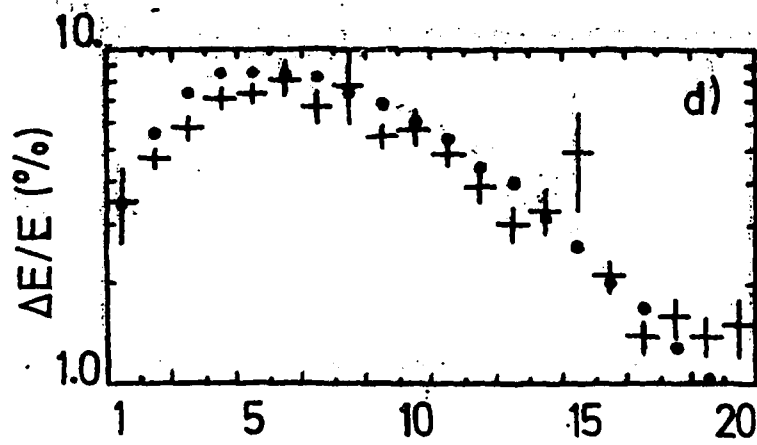
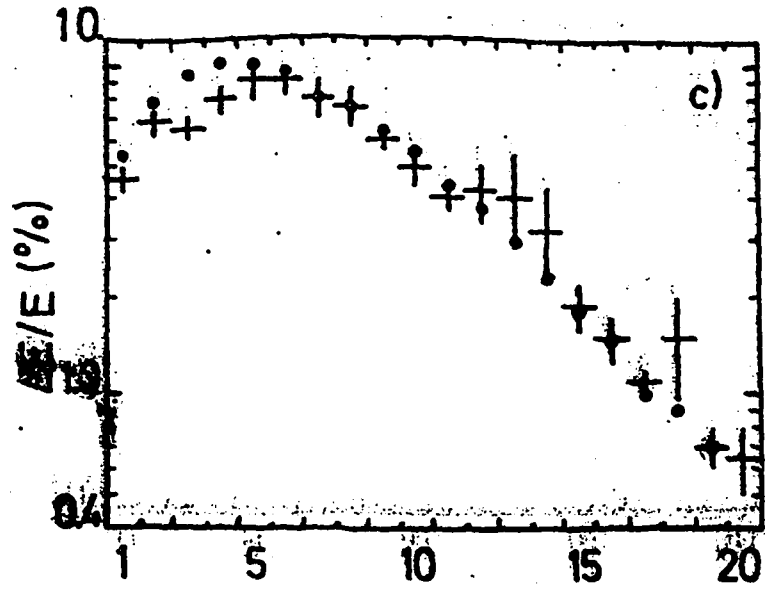


Fig. 1.2

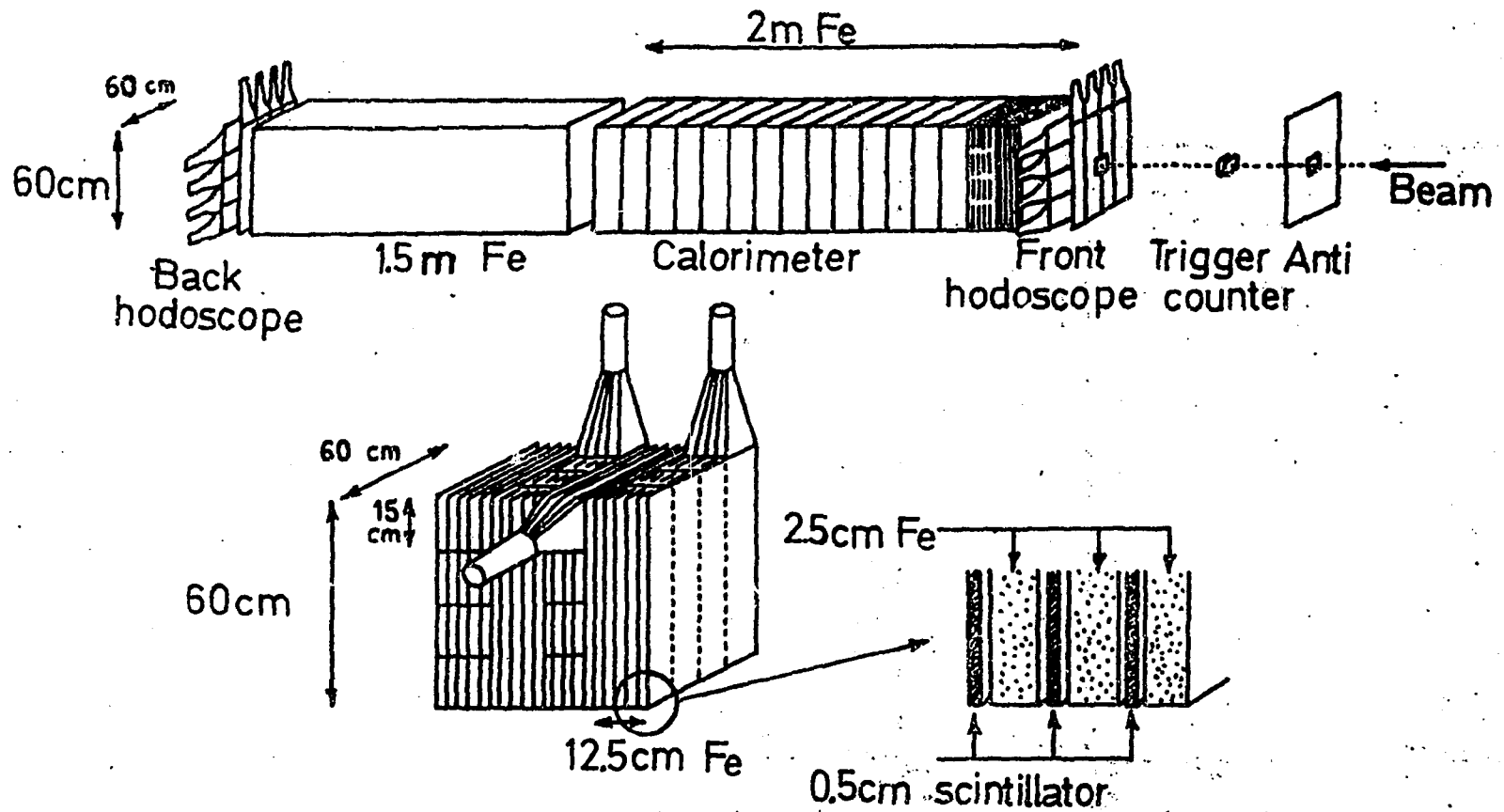
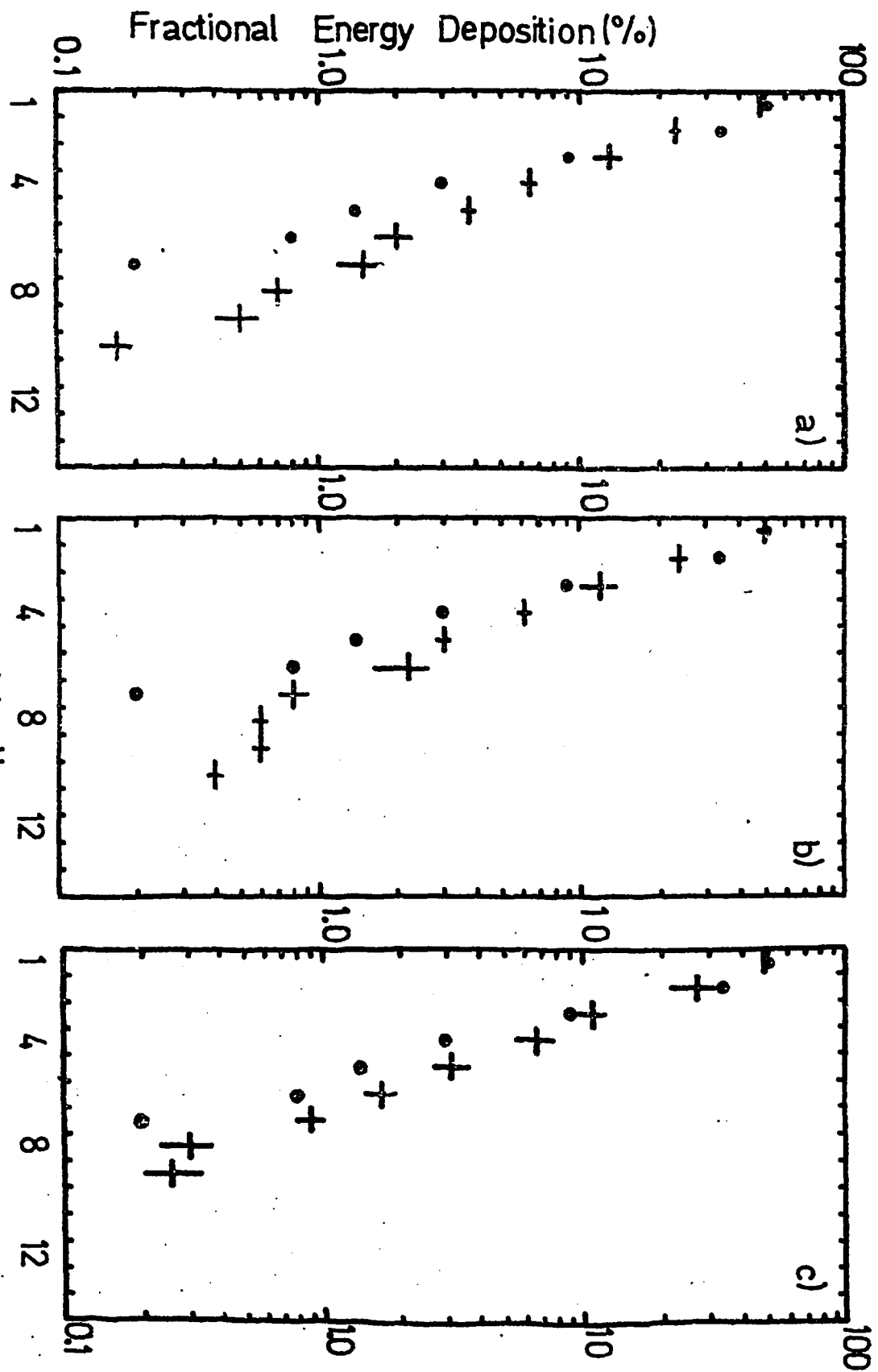


Fig. 1.3



Module #  
Fig. 1.4

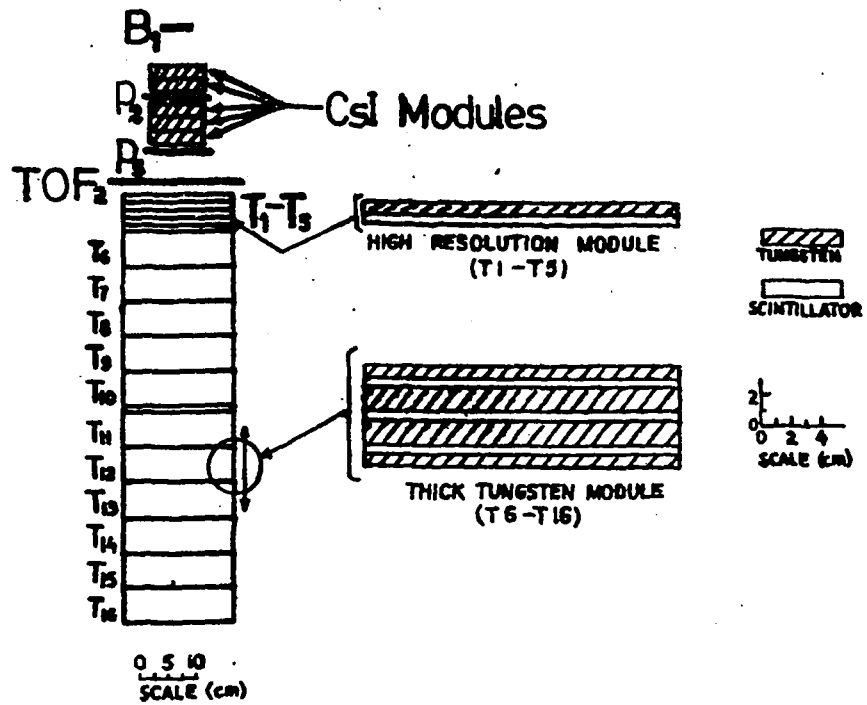
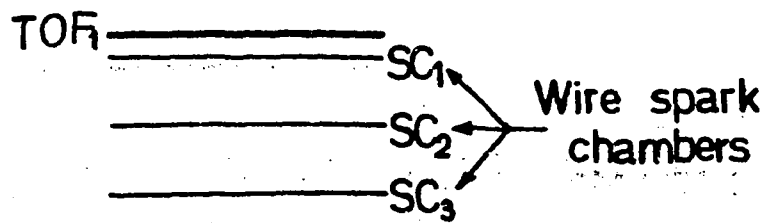


Fig. 1.5

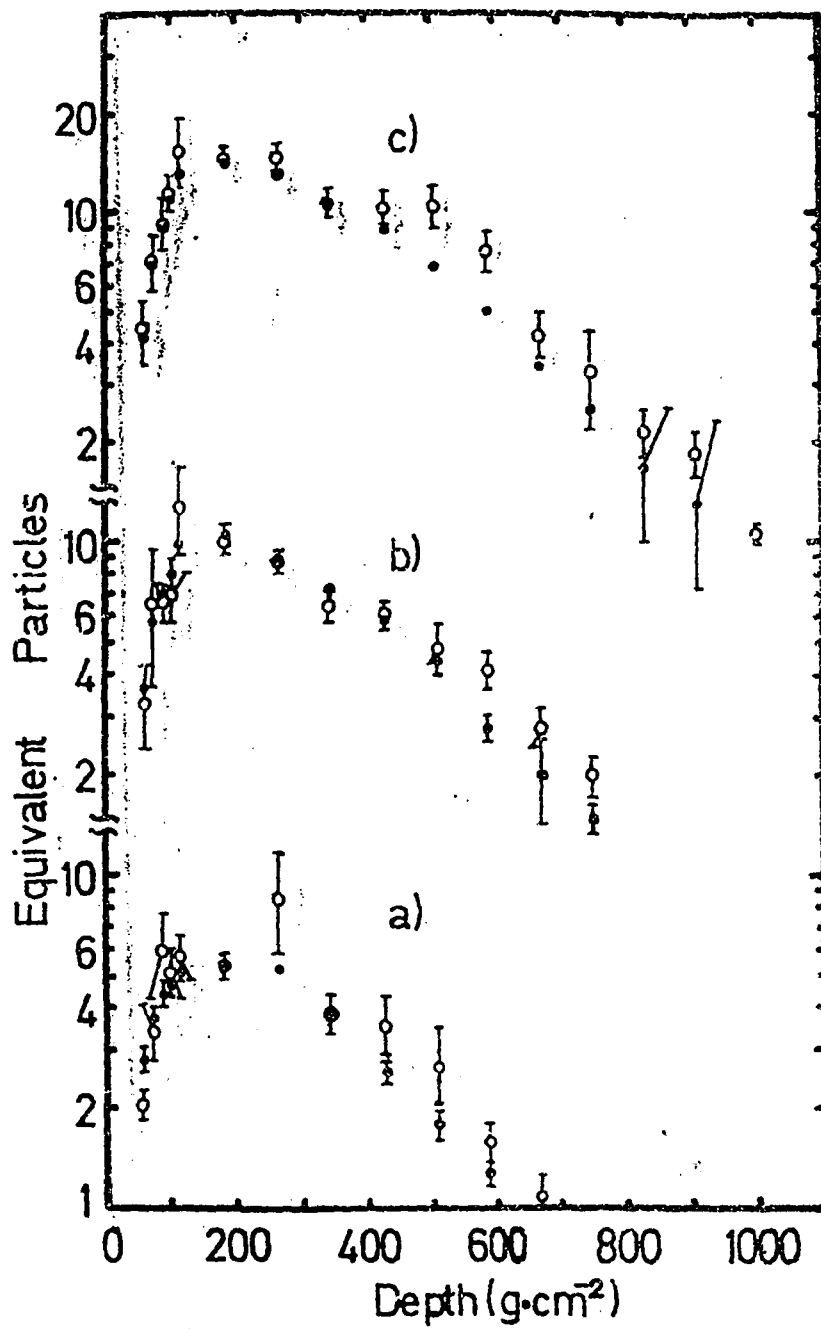


Fig. 1.6

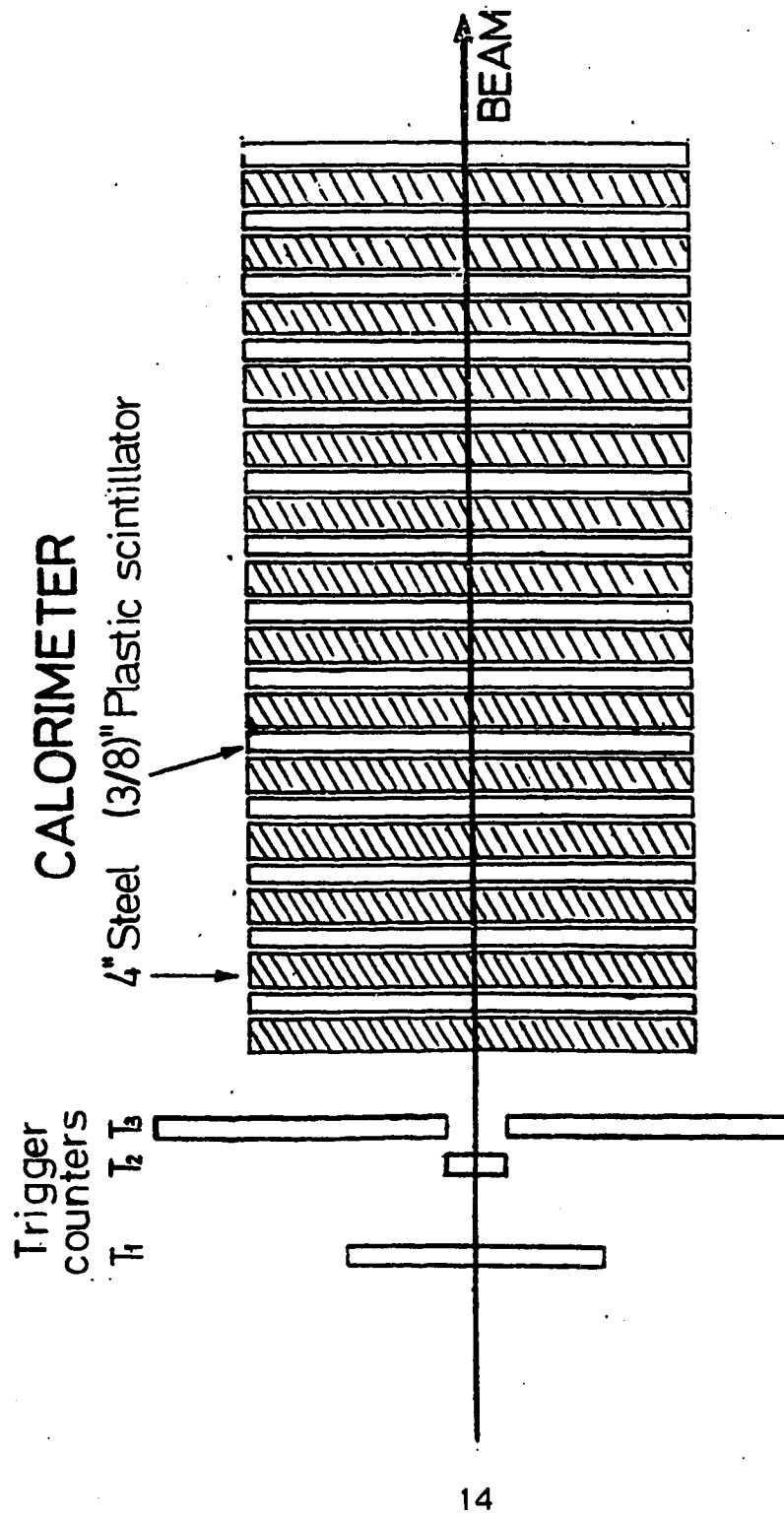
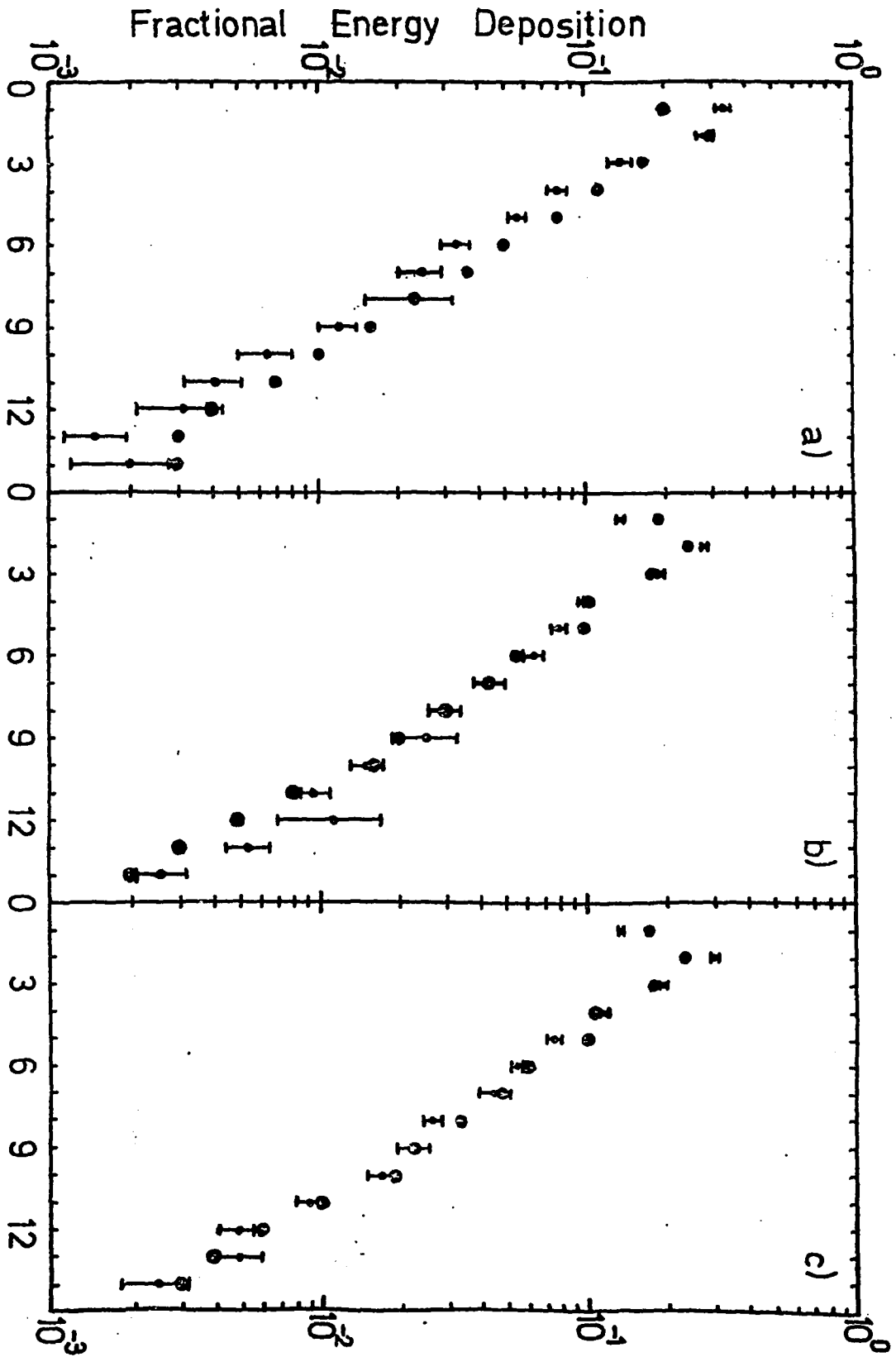


Fig. 1.7



Counter #  
Fig. 1.8

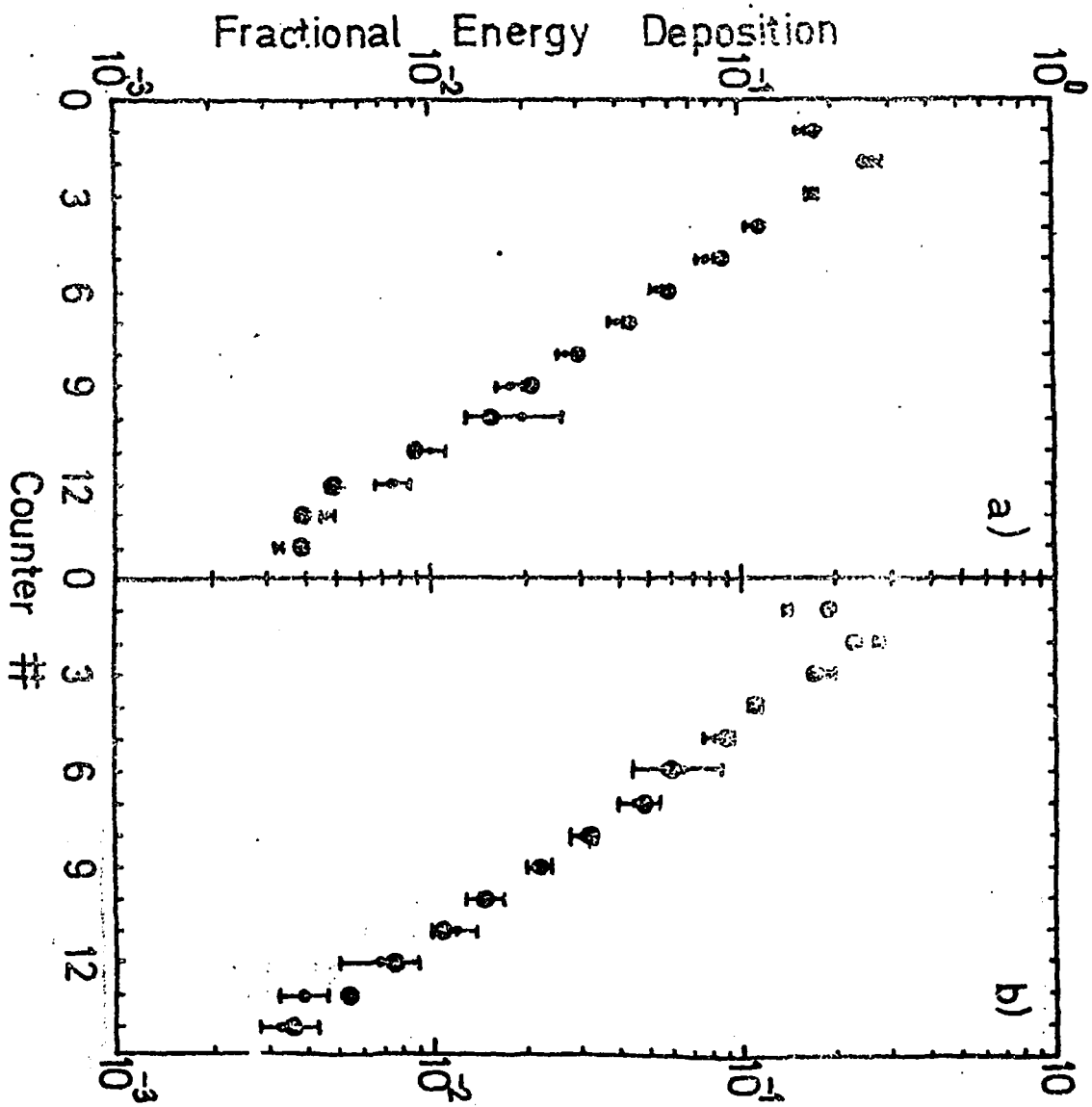


FIG. 19



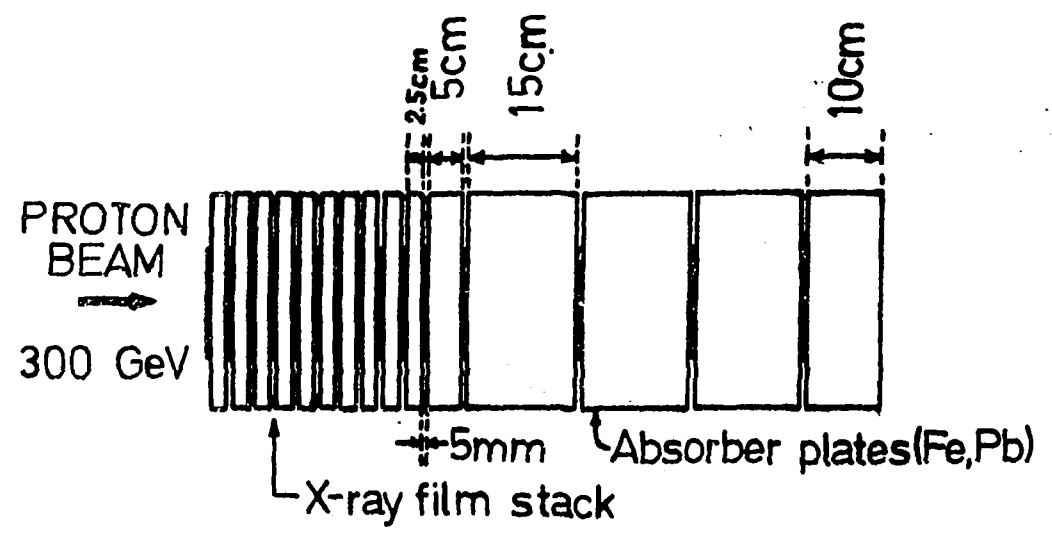


Fig. 1.10

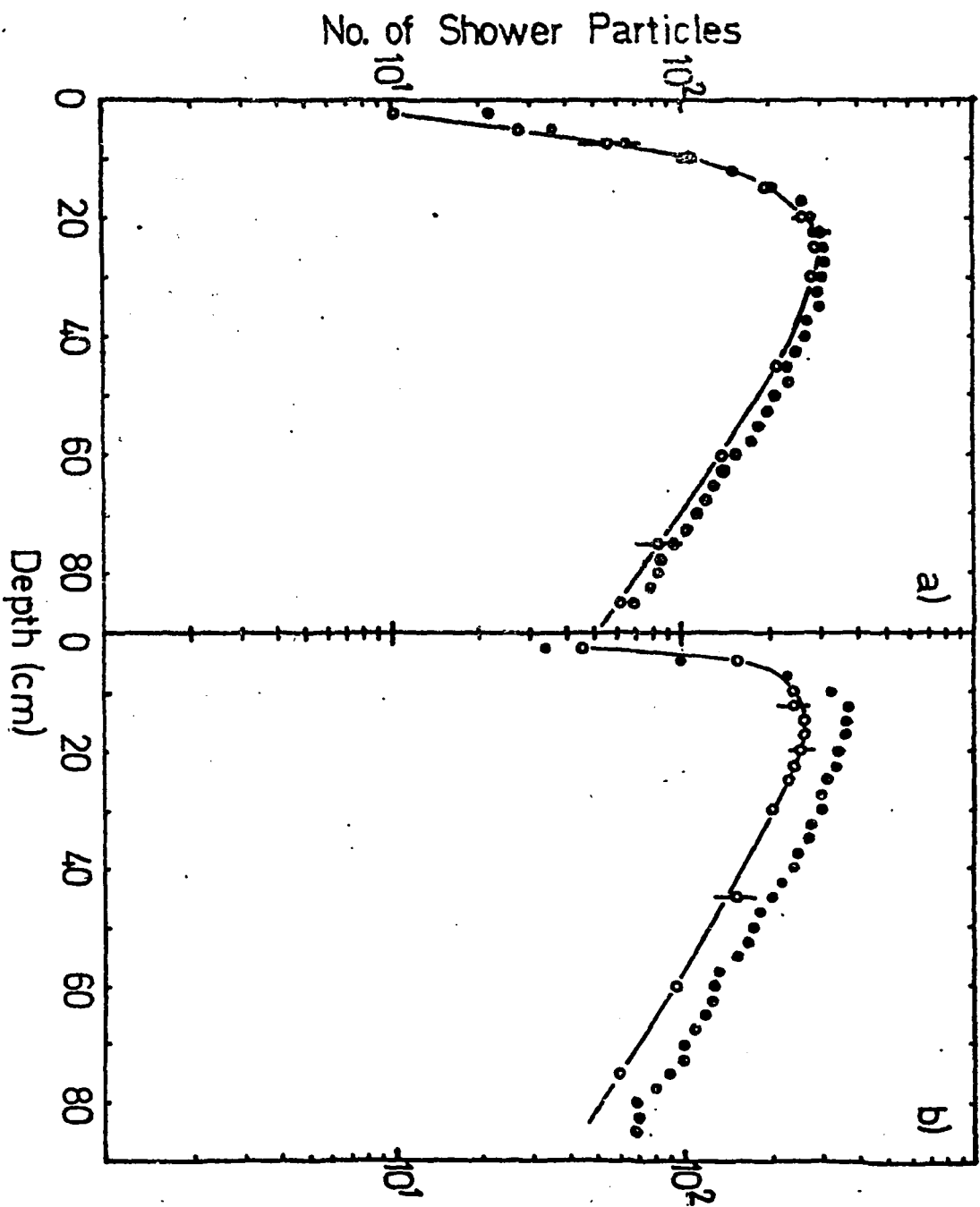


Fig. 1.11

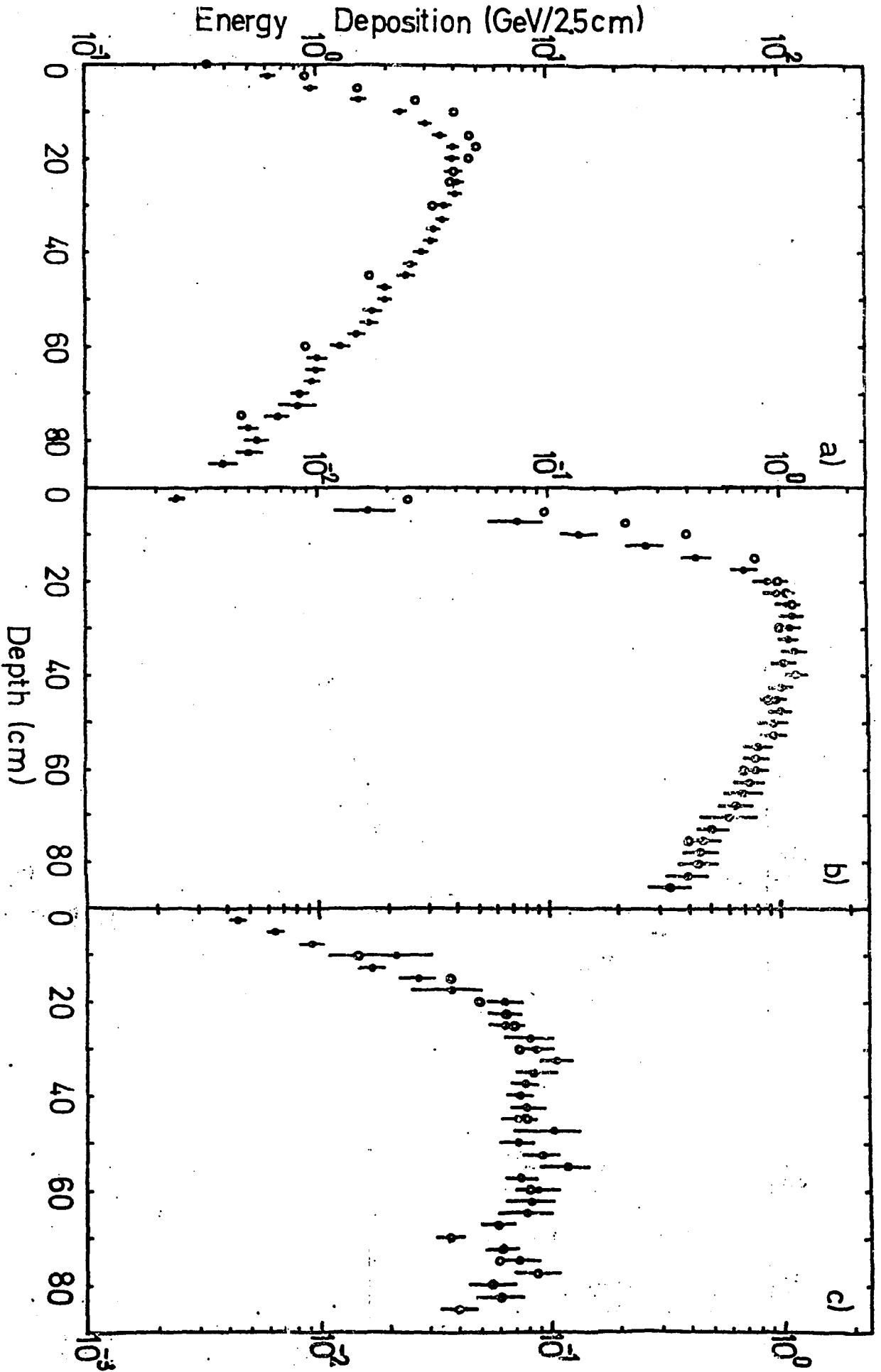


Fig. 1.12

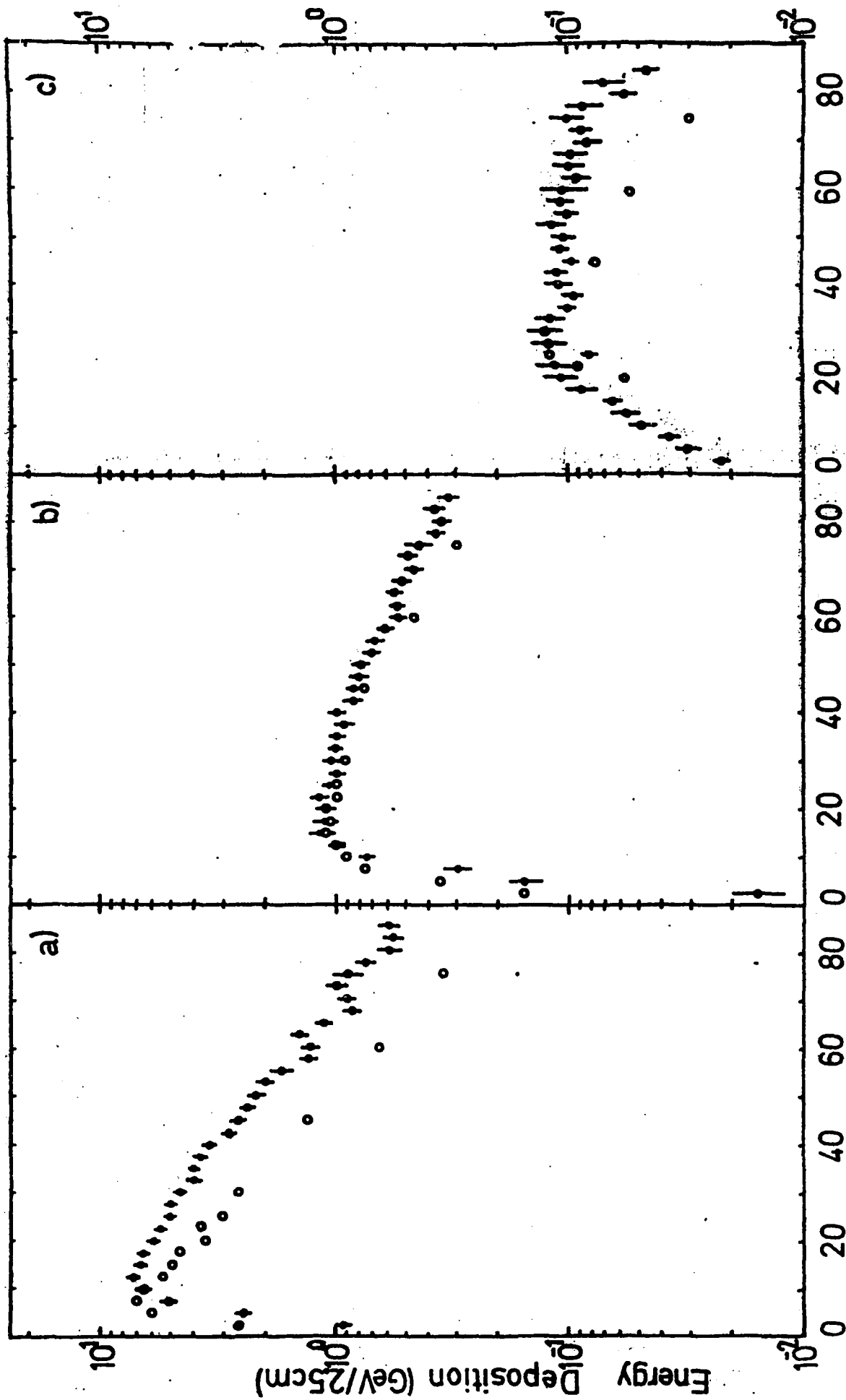


Fig. 1.13

## FIGURE CAPTIONS

[1] Layout of the CHARM prototype calorimeter. Each of the 19 modules consists of  $22\text{gcm}^{-2}$  marble,  $1.5\text{gcm}^{-2}$  Al and  $3\text{gcm}^{-2}$  plastic scintillator.

[2] Fractional energy deposition in the calorimeter modules:  $\ominus$  - exp.[7];  $\oplus$  - MARS10; number of shower histories  $N=10000$ , energy cutoff -  $30\text{MeV}$ , a) -  $E_0 = 1\text{GeV}$ , b) -  $E_0 = 2\text{GeV}$ , c) -  $E_0 = 3\text{GeV}$ , d) -  $E_0 = 5\text{GeV}$ , e)  $E_0 = 6\text{GeV}$ .

[3] Layout of the CDHS calorimeter prototype.

[4] Fraction of the total shower energy detected ( $\ominus$  - [8]) and calculated ( $\oplus$  - MARS10) in each calorimeter module,  $N = 10000$ , the cutoff energy is a)  $10\text{MeV}$ , b) -  $20\text{MeV}$  and c) -  $30\text{MeV}$ .

[5] Scale drawing of the apparatus and the tungsten modules. SC1, SC2 and SC3 are wire spark chambers; TOF1, TOF2, P2, P5 and P7 are plastic scintillators. Each of the modules T1-T5 consist of a  $13\text{gcm}^{-2}$  lead tungsten layer followed by  $6.5\text{mm}$  thick sheet of plastic. Each of the T6-T15 modules consist of 4 layers of tungsten of thickness  $10, 10, 10$  and  $3$  sheets of  $6.5\text{mm}$  thick plastic. The ranges of the tungsten sheets with  $26.3\text{gcm}^{-2}$  of tungsten are respectively: a)  $1.5, 1.5, 1.5$  and  $1.5$ .

[6] The average number of constituent particles in the cascade as a function of rapidity  $y$  and energy  $E$  (  $\ominus$  - exp. data,  $\oplus$  - MARS10). a)  $E_0 = 1\text{GeV}/c$ , cutoff -  $30\text{MeV}$ ; b) -  $10\text{GeV}/c$ , cutoff -  $50\text{MeV}$ ; c) -  $10\text{GeV}/c$ , cutoff -  $30\text{MeV}$ ; d) -  $10\text{GeV}/c$ , cutoff -  $30\text{MeV}$ .

[7] Comparison of the CHARM and CDHS calorimeter.

[8] The fraction of the total energy of negative hadrons in iron as a function of rapidity  $y$  and energy  $E$  (  $\ominus$  - exp. data,  $\oplus$  - MARS10). a) -  $E_0 = 100\text{GeV}$ , b) -  $E_0 = 100\text{GeV}$ , c) -  $E_0 = 100\text{GeV}$ , d) -  $E_0 = 100\text{GeV}$ , e) -  $E_0 = 100\text{GeV}$ , f) -  $E_0 = 100\text{GeV}$ , g) -  $E_0 = 100\text{GeV}$ , h) -  $E_0 = 100\text{GeV}$ , i) -  $E_0 = 100\text{GeV}$ , j) -  $E_0 = 100\text{GeV}$ , k) -  $E_0 = 100\text{GeV}$ , l) -  $E_0 = 100\text{GeV}$ , m) -  $E_0 = 100\text{GeV}$ , n) -  $E_0 = 100\text{GeV}$ , o) -  $E_0 = 100\text{GeV}$ , p) -  $E_0 = 100\text{GeV}$ , q) -  $E_0 = 100\text{GeV}$ , r) -  $E_0 = 100\text{GeV}$ , s) -  $E_0 = 100\text{GeV}$ , t) -  $E_0 = 100\text{GeV}$ , u) -  $E_0 = 100\text{GeV}$ , v) -  $E_0 = 100\text{GeV}$ , w) -  $E_0 = 100\text{GeV}$ , x) -  $E_0 = 100\text{GeV}$ , y) -  $E_0 = 100\text{GeV}$ , z) -  $E_0 = 100\text{GeV}$ .

[9] The fraction of the total energy of positive hadrons in iron as a function of rapidity  $y$  and energy  $E$  (  $\ominus$  - exp. data,  $\oplus$  - MARS10). a) -  $E_0 = 100\text{GeV}$ , b) -  $E_0 = 100\text{GeV}$ , c) -  $E_0 = 100\text{GeV}$ , d) -  $E_0 = 100\text{GeV}$ , e) -  $E_0 = 100\text{GeV}$ , f) -  $E_0 = 100\text{GeV}$ , g) -  $E_0 = 100\text{GeV}$ , h) -  $E_0 = 100\text{GeV}$ , i) -  $E_0 = 100\text{GeV}$ , j) -  $E_0 = 100\text{GeV}$ , k) -  $E_0 = 100\text{GeV}$ , l) -  $E_0 = 100\text{GeV}$ , m) -  $E_0 = 100\text{GeV}$ , n) -  $E_0 = 100\text{GeV}$ , o) -  $E_0 = 100\text{GeV}$ , p) -  $E_0 = 100\text{GeV}$ , q) -  $E_0 = 100\text{GeV}$ , r) -  $E_0 = 100\text{GeV}$ , s) -  $E_0 = 100\text{GeV}$ , t) -  $E_0 = 100\text{GeV}$ , u) -  $E_0 = 100\text{GeV}$ , v) -  $E_0 = 100\text{GeV}$ , w) -  $E_0 = 100\text{GeV}$ , x) -  $E_0 = 100\text{GeV}$ , y) -  $E_0 = 100\text{GeV}$ , z) -  $E_0 = 100\text{GeV}$ .

[10] Arrangement of the CDHS calorimeter chamber.

[11] Number of constituent particles as a function of rapidity  $y$  and energy  $E$  (  $\ominus$  - exp. data,  $\oplus$  - MARS10). a) -  $E_0 = 100\text{GeV}$ , b) -  $E_0 = 100\text{GeV}$ , c) -  $E_0 = 100\text{GeV}$ , d) -  $E_0 = 100\text{GeV}$ , e) -  $E_0 = 100\text{GeV}$ , f) -  $E_0 = 100\text{GeV}$ , g) -  $E_0 = 100\text{GeV}$ , h) -  $E_0 = 100\text{GeV}$ , i) -  $E_0 = 100\text{GeV}$ , j) -  $E_0 = 100\text{GeV}$ , k) -  $E_0 = 100\text{GeV}$ , l) -  $E_0 = 100\text{GeV}$ , m) -  $E_0 = 100\text{GeV}$ , n) -  $E_0 = 100\text{GeV}$ , o) -  $E_0 = 100\text{GeV}$ , p) -  $E_0 = 100\text{GeV}$ , q) -  $E_0 = 100\text{GeV}$ , r) -  $E_0 = 100\text{GeV}$ , s) -  $E_0 = 100\text{GeV}$ , t) -  $E_0 = 100\text{GeV}$ , u) -  $E_0 = 100\text{GeV}$ , v) -  $E_0 = 100\text{GeV}$ , w) -  $E_0 = 100\text{GeV}$ , x) -  $E_0 = 100\text{GeV}$ , y) -  $E_0 = 100\text{GeV}$ , z) -  $E_0 = 100\text{GeV}$ .

solid lines are experiment; ● - MARS10, cutoff - 1Gev for iron, 0.9GeV for lead, N = 10000.

[12] Longitudinal energy deposition in the iron absorber (in arbitrary units) at various radii. a)  $0 < r < 0.5\text{cm}$ , b)  $1\text{cm} < r < 3\text{cm}$ , c)  $10\text{cm} < r < 15\text{cm}$ ; o - experiment, † - MARS10.

[13] The same as in figure 12 for the lead absorber.

## REFERENCES

- [1] A. N. Kalinovski, N. V. Mokhov and Yu. P. Nikitin, Passage of High Energy Particles Through Matter, Energoatomizdat, Moscow, 1985 (in Russian).
- [2] P. A. Aarnio et al., CERN TIS-RP/106 (1983).
- [3] A. Van Ginneken, Fermilab Report, FN-272 (1975).
- [4] N. V. Mokhov, Preprint IHEP 82-166, Serpukhov, 1982.
- [5] N. V. Mokhov and J. D. Cossairt, Fermilab Report, FN-424 (1985).
- [6] P. Gorbunov et al., Preprint ITEP-38, Moscow, 1983.
- [7] P. Gorbunov et al., Preprint ITEP-53, Moscow, 1984.
- [8] R. Abramowicz et al., Preprint CERN-EP/80-188 (1980).
- [9] D. Chesnire et al., NIM, 126, 283 (1975).
- [10] D. Chesnire et al., NIM, 149, 219 (1977).
- [11] D. Chesnire et al., Phys. Rev. D10, 25 (1974).
- [12] D. Chesnire et al., Phys. Rev. D12, 2587 (1975).
- [13] D. Barish et al., NIM, 116, 413 (1974).
- [14] D. Barish et al., NIM 130, 46 (1975).
- [15] Y. Nishiki et al., NIM, A230, 467 (1985).
- [16] S. Olsen and A. Van Ginneken, Fermilab Report, FN-514 (1989).

The manuscript was received 28th Febr. 1991.

Ц. А. АМАТУНИ, Э. А. МАМИДЖАНЫН, А. Н. САНОСЯН  
МОДЕЛИРОВАНИЕ АДРОННЫХ ЛИВНЕЙ МЕТОДОМ МОНТЕ-КАРЛО  
ЧАСТЬ I: СРАВНЕНИЕ РЕЗУЛЬТАТОВ РАСЧЕТОВ ПРОГРАММОЙ MARS 10  
С РЕЗУЛЬТАТАМИ ЭКСПЕРИМЕНТОВ  
(на английском языке)

Редактор А.С. Есян

Технический редактор А.С. Абрамян

---

Подписано в печать 25/11-92г.

Формат 60х84/16

Офсетная печать, 1000 экз.

Тираж 100 экз. № 10

Зак. тип. 062

Индекс 3608

---

Ипечатано в типографии «Азат»

Ереван-36, ул. Коммунальная



**The address for requests:  
Information Department  
Yerevan Physics Institute  
Alikhanian Brothers 2,  
Yrevan, 375036  
Armenia, USSR**